On the SCTC-OCTC Method for the Analysis and Design of Circuits

Stefano Salvatori, *Member, IEEE,* and Gennaro (Rino) Conte

***Abstract*—This paper discusses guidelines that emphasize the relevance of short-circuit- and open-circuit-time constant (SCTC and OCTC, respectively) methods in the analysis and design of electronic amplifiers. It is demonstrated that it is only necessary to grasp a few concepts in order to understand that the two short- and open-circuit cases fall into a single case that can be easily addressed by low-pass and high-pass filters duality. Instead of just teaching the methods as "recipes" for frequency-performance systems analysis, SCTC and OCTC can be efficiently explained in basic analog electronic courses so as to elucidate their underlying principles. The discussion presented here will include two analysis and design examples, used to highlight the benefits gained by the approximated analysis technique, as well as a section that examines the accuracy of the technique.**

***Index Terms*—Low-pass- and high-pass-filter duality, *RC* network reduction, short-circuit and open-circuit time-constant accuracy, short-circuit- and open-circuit-time constant (SCTC and OCTC).**

I. Introduction

ANALOG-CIRCUIT analysis and design received an important contribution from the so-called open-circuit-time constant (OCTC) technique first introduced in the 1960s [1]. In the 1940s, related to the design of wideband vacuum tube amplifiers, Elmore introduced a method to measure the transient response of linear systems [2] that is widely used today for MOS digital-system design [3]–[6]. In analog electronics, the OCTC technique represents a powerful approximate analysis tool for the estimation of the -3 dB high-frequency limit of a circuit. The method applies for accurate hand calculation of the frequency performances of an amplifier. As underlined in several papers [7]–[11], the SCTC and OCTC techniques, although approximate, allow the designer to relate system bandwidth performance to specific circuit elements, assessing their effect on the circuit. Very good discussions and interesting application insights can be found in Thompson's textbook [12]. However, the SCTC and OCTC calculations are usually presented almost like a "recipe" in basic analog electronics textbooks [13], [14]. They can be "mechanically" applied to the circuit under test to estimate the bandwidth of the amplifier. Generally, students are more interested when they understand the principle of the method they are applying; this works best when only a few basic principles have to be remembered. As shown by the examples reported in the final two sections of this paper, the methods allow students to exercise a tight control over their circuit analysis or design, and to develop a real insight into the circuit functionality (especially relevant in basic analog electronics courses).

Manuscript received September 12, 2007; revised May 22, 2008. First published May 05, 2009; current version published August 05, 2009.

The authors are with the Engineering Electronic Department, University Rome Tre, Rome 00146, Italy (e-mail: salvator@uniroma3.it).

Color versions of one or more of the figures in this paper are available online at http://ieeexplore.ieee.org.

Digital Object Identifier 10.1109/TE.2008.928218

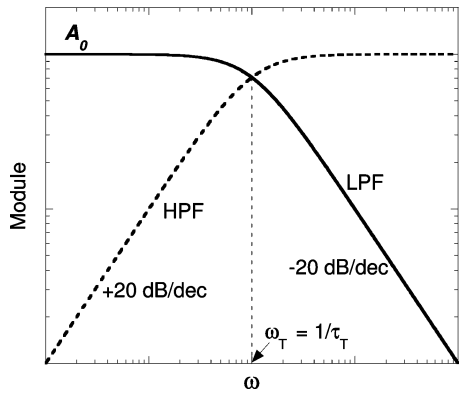

Fig. 1. Frequency response of a first-order LPF (continuous line) and of a first-order high-pass filter (dotted line). The symmetry of the two responses is revealed recalculating the HPF transfer characteristic as a function of $1/\omega$ (see text).

II. A Brief Insight Into the Low-Pass and High-Pass Filters Duality

In the Laplace domain, the transfer function of a first-order low-pass filter (LPF) is simply represented by

$$F_{\mathrm{LPF}}(s) = A_0 \frac{1}{1 + s\tau_T} \tag{1}$$

where A_0 and τ_T are the gain at zero-frequency and the time-constant of the filter, respectively. The latter, given by the circuit elements $R \times C$ product, can be also expressed as its inverse quantity $\omega_T = 2\pi f_T = 1/\tau_T$, in which f_T is the corner frequency where the system gain decreases by 3 dB.

In the same Laplace domain, a high-pass filter (HPF) simply shows the presence of a zero in the origin so that the transfer function modifies to

$$F_{\mathrm{HPF}}(s) = A_0 \frac{s\tau_T}{1 + s\tau_T} \tag{2}$$

which has been written to be exactly comparable to the F_{LPF} function. The intrinsic duality of the two transfer functions is easily revealed by observing the two equations modules as Bode plots, as reported in Fig. 1. "Reading" the HPF response in a *reverse mode* (i.e., from high to low frequencies), the same behavior as that of an LPF is observed: a constant gain followed by a "decrease" of 20 dB per decade of frequency. Again, the two

regions are separated by the $\omega_T = 2\pi f_T$ quantity. Such a similarity is due to the axis nature of the Bode plots. Being plotted on a log scale, reversing an axis indicates the inverse proportion of its variable. This observation is easily confirmed from an analytical point of view. Assuming the new $r = s^{-1}$ independent variable in the HPF transfer function, (2) becomes

$$F_{\mathrm{HPF}}(r) = A_0 \frac{1}{1 + r\omega_T} \tag{3}$$

which is formally identical to the F_{LPF} of (1). (Reversing the s variable does not mean that time is being considered; just that dimension of the r variable is in seconds.) It is worth noting that in such a **reverse mode**, the filter characteristic is summarized by its cut-off frequency ω_T: an inverse proportion in comparison to the τ_T time constant.

These results, derived for first order filters, can be generalized to higher order ones. Assuming the practical situation of n real poles, the LPF transfer function is given by

$$F_{\mathrm{LPF}}(s) = \frac{A_0}{(1 + s\tau_1)(1 + s\tau_2)\ldots(1 + s\tau_n)} \tag{4}$$

where τ_i represents the system time-constant associated with ith real-axis pole.

The previous equation is formally identical to that obtained for an n-order HPF in the $r(= s^{-1})$ variable, and considering the $\omega_i = 1/\tau_i$ constants

$$F_{\mathrm{HPF}}(r) = \frac{A_0}{(1 + r\omega_1)(1 + r\omega_2)\ldots(1 + r\omega_n)}. \tag{5}$$

Here, ω_i constants assume a similar meaning to the LPF τ_i values: they are the system cut-off frequencies, associated with the real-axis poles in the r-variable domain.

Equations (1) and (3) (or (4) and (5) for n real-axis poles) reveal the similarity between the two low-pass and high-pass filters when the s to r variable-change is concerned. This particular behavior provides a first, well-known, insight into the frequency response behavior of a system: in both cases, attention only need to be paid to the poles of its transfer function. When an increase of the s variable is concerned, information is obtained on the upper limit of the frequency response and the poles are expressed by the τ_i time-constants' values. Conversely, in the "reverse fashion", the lower limit of the frequency response is found and the poles are referred to the r variable and expressed in terms of the ω_i values.

The location of the poles of a transfer function is often very difficult to calculate. It is possible to use computer-based circuit simulators to determine the exact location but they give little insight into and intuition for amplifier analysis and design. In the present instance, however, it is of more interest to estimate the bandwidth of the circuit instead of the exact poles' location. As illustrated in Section III, approximated analysis drastically reduces difficulties in evaluating the whole system's time constant and provides the basic idea for the OCTC and SCTC methods.

III. Basic Idea of the Time-Constants Method

Equations (4) or (5) derive from circuits in which n independent capacitors interact with a network composed of resistors and controlled sources. Consider first a system where *RC* elements act as LPFs. Equation (4) can be expanded in the form of (6) at the bottom of the page, in which, due to the particular case here analyzed (n real-axis poles, lying in the left-half plane), the denominator is an n-order Hurwitz polynomial, complete with all positive real-coefficients. The analysis can be simplified by considering just the frequency range in which, compared to that of the midfrequencies, the gain-decrease is lower than or equal to 3 dB (frequencies lower than the roll-off value). In such a case, the previous equation is well approximated by

$$F_{\mathrm{LPF}}(s) \approx \frac{A_0}{1 + (\tau_1 + \tau_2 + \cdots \tau_n)\, s} \tag{7}$$

neglecting, at the dominator, the higher-order s terms. Very good accuracy is achieved when just one time-constant τ_j dominates over all the others, and the analysis is greatly simplified by applying the dominant-pole technique [15]–[17]. In general, a discussion on the accuracy of (7) will be given in Section VI and in the last two sections which show the application of the OCTC approach. Equation (7) means that the LPF is well approximated by a first-order filter with a time constant given by the **sum of the τ_i time constants** associated with individual poles.

Due to the LPF-HPF duality and frequency translation, similar considerations can be applied on the other low-frequency breakpoint limit side. The expanded (5) is well approximated as

$$F_{\mathrm{HPF}}(r) \approx \frac{A_0}{1 + (\omega_1 + \omega_2 + \cdots \omega_n)\, r} \tag{8}$$

neglecting the higher-order r terms: a first-order HPF with a cut-off frequency given by the **sum of the ω_i cut-off frequencies**.

The previous equations show that the analysis of a complex circuit (containing a network of resistors, capacitors, and controlled sources) reduces to finding the *sum* of individual pole time constants (at high-frequency) or cut-off frequencies (in the low frequency range).

In general, performing the poles time-constants calculation is a difficult task, but it can be mathematically demonstrated that

$$F_{\mathrm{LPF}}(s) = \frac{A_0}{1 + (\tau_1 + \tau_2 + \cdots \tau_n)\, s + (\tau_1\tau_2 + \tau_1\tau_3 + \cdots + \tau_1\tau_n + \tau_2\tau_3 + \cdots + \tau_2\tau_n + \cdots + \tau_{n-1}\tau_n)\, s^2 + \cdots + \tau_1\tau_2\ldots\tau_n s^n} \tag{6}$$

their sum is exactly equal to the superposition of the *RC* time constants of the circuit [1], [18]

$$\sum_{i=1}^{n} \tau_i = \sum_{i=1}^{n} R_{Ci} C_i \tag{9}$$

where R_{Ci} represents the equivalent resistive value *seen* by the single C_i capacitor. How can an $R_{Ci}C_i$ element be isolated in the circuit's network? The approach is to treat the system as being composed of capacitors connected to the complex resistive network. Leaving C_i fixed, all the others have to be *disconnected*, and it is possible to evaluate the system response due only to that capacitor. Indeed, by disconnecting a capacitor, both its value and associated time-constant are reduced to zero, pushing to infinity the roll-off contribution of such an *RC* component (well over the 3-dB edge of interest). Similarly, when the HPF behavior is concerned, all the capacitors can be *shorted* (except the one we are analyzing). Shorted capacitors tend to be infinite in value. In this case, their associated low-frequency breakpoints tend toward zero, well below the 3-dB low-frequency edge of the amplifier.

The SCTC-OCTC *recipe* can now be formulated to make a rough estimate of the system bandwidth. This process will be summarized in Section V. In Section IV below, some guidelines will be described for distinguishing between high- or low-pass filtering operated by the RC components of an amplifier.

IV. How to Discriminate Between Low-Pass and High-Pass Capacitors

An obvious step in this approximate analysis includes the identification of capacitors either acting as low-pass or as high-pass elements.

At first, a rule of thumb can be followed by which most of the capacitors *intentionally inserted* in the circuit (i.e., not parasitic) will act as bypass or coupling components, that is high-pass filters. Capacitors in feedback networks cannot with certainty be included in this category. (This situation is one where experience and practice would really help the analysis.) Conversely, all the parasitic capacitances, related to the small-signal models of active devices, will act to decrease the upper limit of the amplifier's frequency response. In such a case, they will act as low-pass elements in the system analysis.

For beginners trying to identify the function of various capacitors, a few guidelines can be provided.

The analysis can start by focusing attention on the capacitors intentionally included in the system. The circuit can be analyzed without using the equivalent transistor small-signal model. These active devices can be considered just as amplification-boxes. (When using this method, it is important to have a concise knowledge of the main characteristics of the fundamental transistor configurations.) Obviously, also in presence of the input ac signal, the effect of all the sources, considered as constant components (independent dc voltage- and current-sources), can be cancelled. It can be easily verified that a capacitor, when shorted, would increase the signal transfer from the input to the output. This change in signal transfer also includes the gain increase of an amplifier stage. This analysis can be confirmed by opening the capacitor terminals and by observing a decrease of the ac signal transfer or stage gain. To put it concisely, if a capacitor increases either the signal transfer from the input to the output or the gain of the amplifier, it will act as a **high-pass-frequency element**. Conversely, if a complementary behavior is observed, in conjunction with the resistive network the capacitor interacts with, *RC* **low-pass filtering** is concerned. (All the above considerations obviously have to be reversed from the designer's point of view: coupling and bypass capacitors will be inserted in paths where an increase of the signal transfer or of the amplification would be guaranteed.)

As far as parasitic capacitances are concerned, since they are considered in the small signal model of a device macroscopically to describe the speed limits of the component, the equivalent *RC* elements will act as low-pass filters. Indeed, by shorting one of these capacitors, and by leaving open the others, a decrease either in the transferred signal amplitude or in the gain of the amplifier stage will be observed.

V. The SCTC-OCTC "Recipe"

As a final step of this discussion, the recipe for the SCTC-OCTC analysis technique can be formulated. In particular, as shown in Section III, in the high frequency regime, the time constants associated with the different $\tau_i = R_{Ci}C_i$ elements can be found. All the coupling and bypass components have to be shorted. The particular τ_i quantity is calculated by opening all the other capacitors. Finally, as stated in the discussion related to (7), the low-pass behavior of the system is approximated by a first-order LPF, whose time constant τ_T is given by the sum of all the calculated $R_{Ci}C_i$ products. This observation means that the system cut-off frequency is close to the value

$$f_{3\ \mathrm{dB\_high}} = \frac{1}{2\pi\tau_T} = \frac{1}{2\pi \sum R_{Ci}C_i}. \tag{10}$$

Due to the complementary behavior discussed in Section II and the suggestions of Section III, the low-frequency breakpoint values associated to the different $R_{Ci}Ci$ elements can be evaluated by shorting all the other by-pass capacitors (low-pass capacitors being kept as open circuits). The high-pass behavior of the circuit is approximated by a first-order HPF with a cut-off frequency $f_{3\ \mathrm{dB\_low}}$ simply given by the sum of f_i values according to

$$f_{3\ \mathrm{dB\_low}} = \sum f_i = \frac{1}{2\pi} \sum \frac{1}{R_i C_i}. \tag{11}$$

VI. On the Accuracy of the SCTC-OCTC Analysis

How accurate is the bandwidth estimate? Such a question may appear moot because of the intrinsic approximative nature of the SCTC-OCTC method. Leaving to one side these *philosophical implications*, it would nevertheless be useful to calculate the order of magnitude of the error obtained when an n-order system, (6), is approximated by a first-order one, (7). Moreover, the discussion sheds light on the frequency range for which

the analysis yields a good approximation of the amplifier bandwidth.

For the higher order terms, since only frequencies up to the -3 dB corner-value are of interest, a relative low-frequency regime can be assumed. This assumption means that the s^2 term of (6) will introduce most of the error in the approximation. This term is rewritten here collecting terms containing the $\tau_T = \Sigma\tau_i$ component (the sum of the pole time-constants which represents the estimate of the circuit response speed)

$$s_{2-\text{term}} = s^2\left[\tau_1(\tau_T-\tau_1)+\tau_2(\tau_T-\tau_1-\tau_2)+\cdots +\tau_{n-1}(\tau_T-\tau_1-\tau_2-\cdots-\tau_{n-1})\right] \quad (12)$$

whose maximum can be obtained by calculating the maximum of each of its addenda. Starting from the first τ_1 term, towards the last term, gives: see (13) at the bottom of the page. So, for the n-order polynomial at the denominator of (6), the s^2 coefficient assumes a maximum value given by

$$\begin{aligned} s_{2-\text{coeff}}^{\max} &= \tau_T^2\left[\left(\frac{1}{2}\right)^2+\left(\frac{1}{4}\right)^2+\cdots+\left(\frac{1}{2^{n-1}}\right)^2\right] \\ &= \tau_T^2\sum_{i=1}^{n-1}\frac{1}{2^{2i}} = \tau_T^2\varepsilon_{n-\max}. \end{aligned} \quad (14)$$

As an example, for a second-order LPF, $n=2$ and $\epsilon_{n-\max} = 0.25$. Such a value simply states that the worse case condition for the OCTC analysis is when the two poles are coincident. Indeed, substituting $\epsilon_{n-\max} = 0.25$, the transfer function is given by

$$F_{\text{LPF2}}(s) = \frac{1}{1+s\tau_T+0.25s^2\tau_T^2} = \frac{1}{(1+0.5s\tau_T)^2} \quad (15)$$

with the $\tau_1 = \tau_2 = 0.5\tau_T$ solution for poles' calculation. The error incurred by assuming $1/\tau_T$ as the cut-off frequency by the OCTC method can be found by evaluating the exact value of (15) by

$$\left|\frac{1}{(1+0.5j\omega_{3\text{ dB}}\tau_T)^2}\right| = \frac{1}{\sqrt{2}} \quad (16)$$

whose solution gives

$$\omega_{3\text{ dB}} = \frac{2\sqrt{\sqrt{2}-1}}{\tau_T} \cong \frac{1.29}{\tau_T} \quad (17)$$

stating that, in a second-order LPF, the OCTC method, neglecting the unique high-order s^2 term in the second-order LPF, underestimates the bandwidth at maximum by 22.3% $(=1-1/1.29)$ over the exact $\omega_{3\text{ dB}}$ value.

When n increases, (14) furnishes

$$\begin{aligned} \varepsilon_{n-\max} &= \frac{1}{2^2}+\frac{1}{2^4}+\frac{1}{2^6}+\cdots \\ &= \frac{1}{2^2}\left(1+\frac{1}{2^2}+\frac{1}{2^4}+\frac{1}{2^6}+\cdots\right) \\ &\Rightarrow \varepsilon_{n-\max} \approx \frac{1}{4}(1+\varepsilon_{n-\max}) \end{aligned} \quad (18)$$

where the last equation is exact for $n\to\infty$, so that $\epsilon_{n-\max}\to 1/3$. To evaluate the OCTC accuracy, neglecting higher order terms, the following equation:

$$\left|1+j\omega_{3\text{ dB}}\tau_T-\frac{1}{3}\omega_{3\text{ dB}}^2\tau_T^2\right| = \sqrt{2} \quad (19)$$

can be solved. Previous equation gives $\omega_{3\text{ dB}} \approx 1.36/\tau_T$ and indicates a maximum underestimation of 27%. Although the calculated error values may appear high, they are practically comparable with tolerances usually found for active components.

From the previous result, the high frequency limit can be evaluated for which the approximative analysis should be considered still valid. The Bode-plot of the module of an n-order LPF transfer function intersects the first-order OCTC response approximately at the frequency where

$$\left|1+j\omega\tau_T-\omega^2\tau_T^2\varepsilon_{n-\max}\right| = \left|1+j\omega\tau_T\right| \quad (20)$$

whose solution gives

$$\omega = \sqrt{\frac{2}{\varepsilon_{n-\max}}}\frac{1}{\tau_T}. \quad (21)$$

Based on the results shown above $(\varepsilon_{n-\max} = 1/3)$, the $\sqrt{6}/\tau_T$ value can be considered the limit beyond which the approximation would begin to fail.

Complementary results are verified when the low frequency cut-off of the amplifier is concerned. In particular, the SCTC approximation can be considered valid if $\omega \geq \omega_{\text{est}}/\sqrt{6}$, whereas the underestimate of the low-frequency breakpoint is again about 27% when $n>2$ is concerned.

VII. An Analysis Case Study: Third-order LPF

To discuss the application of the OCTC method, the example reported in Fig. 2(a) of a third-order LPF will be analyzed.

The transfer function of the circuit can be exactly calculated by applying Thevenin's theorem "three times" (moving from the R1-C1 network towards the R3-C3 components at the output), or by writing the node equations of the circuit. (The latter will be useful to calculate the eigenvalues of the conductance matrix to

$$\begin{aligned} \max\left[\tau_1(\tau_T-\tau_1)\right] = \frac{\tau_T}{2}\frac{\tau_T}{2} \Rightarrow \max\left[\tau_2\left(\tau_T-\frac{\tau_T}{2}-\tau_2\right)\right] = \frac{\tau_T}{4}\frac{\tau_T}{4} \Rightarrow \dots \\ \dots \Rightarrow \max\left[\tau_{n-1}\left(\tau_T-\frac{\tau_T}{2}-\frac{\tau_T}{4}-\cdots-\tau_{n-1}\right)\right] = \left(\frac{\tau_T}{2^{n-1}}\right)^2. \end{aligned} \quad (13)$$

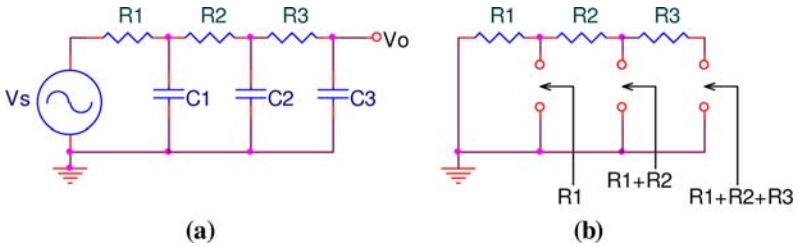

Fig. 2. (a) A third-order LPF used to apply the OCTC method in the analysis of a circuit. (b) The resistive network used to find the components seen by each capacitor.

find the poles' exact location.) Finally, the input-output voltage ratio is given by

$$\frac{v_0}{v_s} = \Big[1 - \omega^2(\tau_1\tau_2 + \tau_1\tau_3 + \tau_2\tau_3 + \tau_{12}\tau_3 + \tau_1\tau_{23}) + j\omega(\tau_1 + \tau_2 + \tau_3 + \tau_{12} + \tau_{13} + \tau_{23}) - j\omega^3\tau_1\tau_2\tau_3\Big]^{-1} \quad (22)$$

where $\tau_i = R_iC_i$ and $\tau_{ij} = R_iC_j (i, j = 1 \ldots 3)$.

The use of the OCTC method involves the calculation of the time-constants associated to each capacitor. As depicted in Fig. 2(b), the evaluation of the resistive component seen by each capacitor is given by

$$R_{C1} = R_1, \quad R_{C2} = R_1 + R_2, \text{ and } R_{C3} = R_1 + R_2 + R_3 \quad (23)$$

from which the open-circuit time-constant is estimated as the sum of the found three terms

$$\tau_T = R_1C_1 + (R_1 + R_2)C_2 + (R_1 + R_2 + R_3)C_3. \quad (24)$$

It is worth noting that the calculated τ_T is formally identical to that of the $j\omega$ term of (22) as expected by (9). The high-frequency roll-off is finally evaluated with (24) by

$$f_T = \frac{1}{(2\pi\tau_T)}. \quad (25)$$

The worse case condition for the OCTC accuracy might be expected to obtain when the time-constants of (24) assume the same value. (Indeed, if the system had a dominant pole, the frequency response, close to the -3 dB range, would be well approximated by the first-order LPF assumed by the OCTC analysis.) Without loss of generality, the R_i values are considered equal to an identical R quantity so that $\tau_{Ci} = R_{Ci}C_i = RC/3$ (with $i = 1 \ldots 3$) are fixed. This equality is guaranteed by choosing

$$C_1 = \frac{C}{3}, \quad C_2 = \frac{C}{6}, \text{ and } C_3 = \frac{C}{9} \quad (26)$$

and, by (24), $\tau_T = RC = \tau$. In Fig. 3(a), the transfer function behavior of the circuit (continuous line) is compared to that approximated by the OCTC analysis (dotted line). Due to the assumptions on the *RC* values of the circuit, the -3 dB bandwidth-estimate using the OCTC method is $1/\tau$. Conversely, the exact value is close to $1.2/\tau$ with a relative error of about 17%.

Without reference to the circuit of Fig. 2, when the ideal case of three coincident poles is concerned, the relative bandwidth error approaches the 34% value (as shown by the $|1 + j\omega\tau/3|^{-3}$ behavior reported as a dotted-line curve in the same figure with a cut-off around $1.5/\tau$). Well above the value of 27%, as calculated by evaluating just the s^2-coefficient contribution (Section VI), this result underlines that while a fairly good accuracy in OCTC is expected for systems having up two coincident dominant poles, for systems with higher number of coincident poles the accuracy is less good.

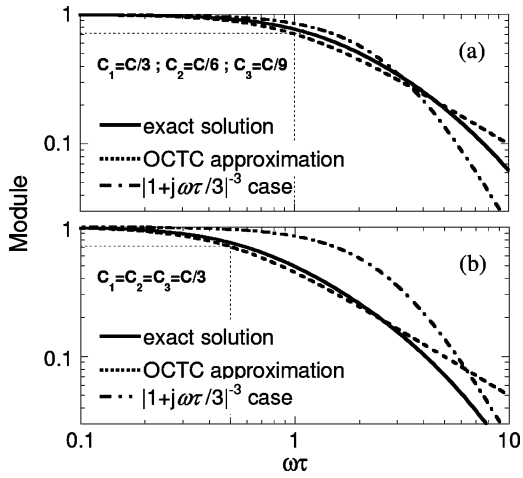

Fig. 3. Module of the frequency response of the third-order filter of Fig. 2 for two different sets of capacitor values (see text). In (a), the worse case condition for the OCTC accuracy is analyzed (see the C_i values reported as inset). In (b), the response when all three capacitors assume the same $C/3$ value is considered. In both cases, the light dotted-line shows the cut-off estimated by the OCTC analysis.

Finally, the case in which all the capacitors have the same $C/3$ value can be analyzed. As shown in Fig. 3(b), the response of such a circuit approaches the $|1+j\omega\tau/3|^{-3}$ behavior at frequencies much greater than the cut-off f_T value. Abscissa values have been normalized to the same $R \times C$ quantity used for data of Fig. 3(a), so that now the OCTC -3 dB-bandwidth is equal to the $0.5/\tau$ value. It can be verified that the OCTC method underestimates the exact bandwidth by 14%, emphasizing yet the benefit of time-constant analysis when a dominant pole condition is concerned.

VIII. A Design Case Study: Cascode Amplifier

As an example of the application of the discussed method, this section treats the possible design of a wideband amplifier for a communication link. The amplifier gain has to be at least 100, with a high-frequency roll-off higher than 5 MHz and a low-frequency breakpoint around 1 kHz. Moreover, driven by a source resistance of the order of 2500 Ω and loaded by an impedance equal to $1\ \text{k}\Omega||10\ \text{pF}$, the circuit has to act as a buffer.

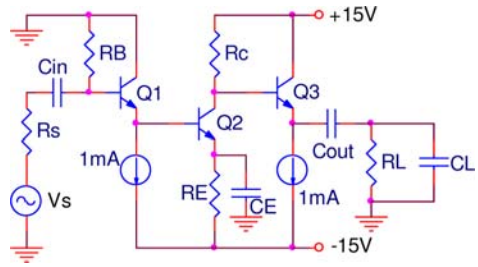

Fig. 4. Schematic of the possible high gain, wideband amplifier based on a common-emitter stage Q2 with buffered input and output.

A ± 15 V power supply is available and the power consumption has to be lower than 150 mW.

A non-inverting amplifier, based on a fast-wideband operational amplifier (with a gain-bandwidth product higher than 500 MHz) could easily meet these requirements. One of the great challenges of analog circuit design, however, is to maximize the performance of a system given any particular set of devices. So, for the example described here, the amplifier will be built by using a few inexpensive 2N3904 general purpose NPN transistors.

Due to the above-mentioned high-gain requirement, the amplifier can be based on a common-emitter transistor configuration. For the buffers, two common-collector stages will be included as input- and output-stages of the amplifier, as shown in Fig. 4.

To meet the power consumption requirements, the collector currents for both the two Q1 and Q3 emitter-follower stages will be fixed at 1 mA. A 2-mA current will be assumed for the intermediate common-emitter transistor Q2, however, both because it is the main amplifier stage, and to achieve a higher current gain. Since this example focuses on the application of the OCTC method to estimate the small-signal bandwidth of the amplifier, any discussion on the biasing circuitry will be omitted. Some details of the biasing circuitry will be found later, by looking at the schematic of the prototype used to verify the real circuit performances.

Neglecting any loading effect between stages and at the input- and output-connections, and assuming unity voltage-gain for emitter followers, the gain equation is well approximated by

$$A_V \approx -g_{m2} R_C \tag{27}$$

where

$$g_{m2} = \frac{I_C}{V_T} = 0.077\,\Omega^{-1} \tag{28}$$

is the Q2 transconductance. Using (27), the minimum R_C value that achieves $A_V \geq 100$ is 1300 Ω. In order to ensure a little bit of extra gain, an $R_C = 1500\ \Omega$ will be assumed.

For small-signal analysis, the simplified π model for each transistor will be used, where

$$r_\pi = \frac{h_{fe}}{g_m} \text{ and } C_\pi = \frac{g_m}{2\pi f_T} - C_\mu \tag{29}$$

represent the resistive and capacitive components of the base-emitter impedance, respectively, whereas $C\mu$ is the feedback base-collector capacitance, h_{fe} and g_m are the BJT current-gain and transconductance, respectively, and f_T the unity-gain cut-off frequency. (Feedback $r\mu$ and output r_O resistors are neglected in the approximate, first cut, analysis.) As depicted in the device datasheet [19], $C\mu$ capacitance strongly depends on the V_{CE} voltage amplitude. In this simplified study, a value of 2 pF and an $f_T = 300$ MHz for each 2N3904 are assumed. Moreover, at the aforementioned biasing currents, the h_{fe} small-signal current gain can be evaluated to be around 150. Finally, for the base-resistance, a realistic value $r_x = 100\ \Omega$ is considered.

Redrawing the circuit in the ac high-frequency regime, the 3-dB roll-off will be estimated using the OCTC method. Following the suggestions given in Section IV, C_{in}, C_{out}, and C_E capacitors have been *intentionally* inserted to act as high-pass elements. Indeed, at relatively high frequencies, C_{in} and C_{out} capacitors allow coupling for input and output signals, respectively. Conversely, when signal-frequency increases, C_E makes a bypass toward ground for the Q2-emitter, zeroing any feedback delivered by R_E and increasing the Q2-stage gain. As illustrated below, their values have been chosen according to the required low-frequency breakpoint of 1 kHz. For the analysis in the high-frequency regime, bypass capacitors have been shorted and the equivalent ac-model of the circuit is shown in Fig. 5. The calculated values for small-signal parasitic elements of BJTs are reported in the same figure.

To apply the OCTC method, all the capacitors are *disconnected*. The resistance value each capacitor sees can be calculated by circuit inspection. As an example, the equivalent resistive-network $C\pi_1$ sees is reproduced in Fig. 6(a). Replacing $C\pi_1$ with a V_x test signal, Thevenin's theorem can be applied in order to calculate the V_x/i_x ratio. With $R_{\text{in2}} = r_{\pi 2} + r_{x2}$, by node equations, it is found

$$v_x = \left(i_x - \frac{v_x}{r_{\pi 1}}\right)(r_{x1} + R_S) - \left(g_{m1} v_x - i_x + \frac{v_x}{r_{\pi 1}}\right) R_{\text{in2}} \tag{30}$$

which can be solved to find the open-circuit resistance and time-constant of $C\pi_1$

$$R_{C\pi 1} = \frac{v_x}{i_x} = r_{\pi 1} \frac{r_{x1} + R_S + R_{\text{in2}}}{r_{x1} + r_{\pi 1} + R_S + (1 + h_{fe}) R_{\text{in2}}} \approx 58.1\Omega \tag{31}$$

$$\tau_{C\pi 1} = R_{C\pi 1} C_{\pi 1} \approx 1.06\ \text{ns}. \tag{32}$$

To find the open-circuit resistance for $C\mu_1$, the equivalent schematic of Fig. 6(b) can be used. The test voltage, V_x, is now referred to ground, so circuit inspection immediately gives

$$R_{C\mu 1} = (r_{x1} + R_S) || [r_{\pi 1} + (1 + h_{fe}) R_{\text{in2}}] \approx 2580\ \Omega \tag{33}$$

$$\tau_{C\mu 1} = R_{C\mu 1} C_{\mu 1} \approx 5.16\ \text{ns}. \tag{34}$$

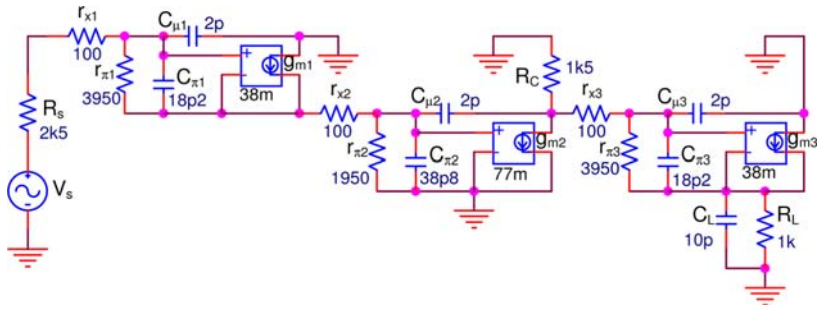

Fig. 5. Equivalent schematic in the high-frequency regime of the circuit of Fig. 4. The simplified π model is used for the BJTs.

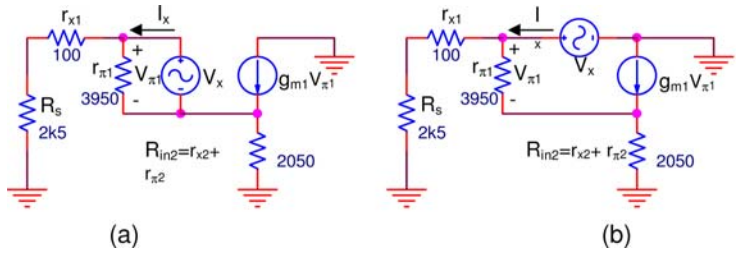

Fig. 6. Equivalent resistive network seen by $C\pi_1$ (a) and $C\mu_1$ (b). Replacing the capacitors V_x represents the test signal in the application of Thevenin's theorem.

Applying the same method to all the parasitic capacitors, the results are summarized by the following equations:

$$R_{C\pi 2} = r_{\pi 2} || \left[r_{x2} + \frac{r_{x1} + r_{\pi 1} + R_S}{1 + h_{fe}} \right] \approx 133.6\ \Omega \Rightarrow \tau_{C\pi 2} \approx 5.18\ \text{ns} \quad (35)$$

$$R_{C\mu 2} = R_{C\pi 2} + (R_C || R_{\text{in3}})(1 + g_{m2} R_{C\pi 2}) \approx 16.9\ \text{k}\Omega \Rightarrow \tau_{C\mu 2} \approx 33.80\ \text{ns} \quad (36)$$

with $$R_{\text{in3}} = r_{x3} + r_{\pi 3} + (1 + h_{fe}) R_L (\approx 155\ \text{k}\Omega) \quad (37)$$

$$R_{C\pi 3} = r_{\pi 3} \frac{r_{x3} + R_C + R_L}{r_{\pi 3} + r_{x3} + R_C + (1 + h_{fe}) R_L} \approx 65.6\ \Omega \Rightarrow \tau_{C\pi 3} \approx 1.19\ \text{ns} \quad (38)$$

$$R_{C\mu 3} = (r_{x3} + R_C) || [r_{\pi 3} + (1 + h_{fe}) R_L] \approx 1584\ \Omega \Rightarrow \tau_{C\mu 3} \approx 3.17\ \text{ns} \quad (39)$$

$$R_{CL} = R_L || \frac{r_{x3} + r_{\pi 3} + R_C}{1 + h_{fe}} \approx 35.5\ \Omega \Rightarrow \tau_{CL} \approx 0.35\ \text{ns}. \quad (40)$$

The open-circuit time constants, calculated by means of reported resistances, give

$$\tau_T = \tau_{C\pi 1} + \tau_{C\mu 1} + \tau_{C\pi 2} + \tau_{C\mu 2} + \tau_{C\pi 3} + \tau_{C\mu 3} + \tau_{CL} \approx 49.9\ \text{ns} \quad (41)$$

and a cut-off frequency

$$f_{3\ \text{dB}} = \frac{1}{2\pi \tau_T} \approx 3.19\ \text{MHz}. \quad (42)$$

SPICE simulation of the circuit-model of Fig. 5 furnishes a -3 dB bandwidth of about 4.2 MHz, showing the OCTC estimate to be a good result. The power of the OCTC analysis is underlined by the possibility of **identifying** the capacitance which dominates in the cut-off frequency. In the case discussed here, due to the well-known Miller effect [20] exhibited by Q2, the time constant associated with the capacitor $C\mu_2$ represents the major limiting factor in the overall frequency response. The Miller effect can be drastically reduced by decreasing the voltage gain of transistor Q2, by using the *cascode* configuration of Fig. 7. The controlled output current of Q1 is buffered by the common-base transistor Q4. The overall voltage gain is again around $|g_{m2} R_C|$, assuming Q4 provides approximately unity current-gain. Moreover, the resistance looking at the emitter of Q4 is very low, so the voltage gain of Q2 strongly decreases, hence reducing the Miller effect.

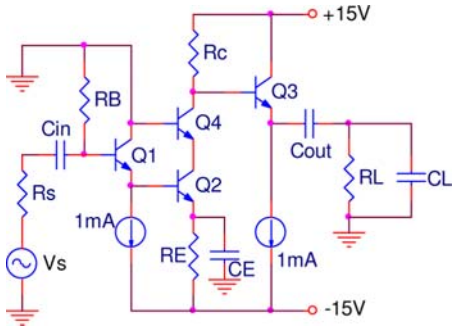

Fig. 7. Schematic of the cascode stage to increase the bandwidth of the amplifier.

The equivalent ac-model is reported in Fig. 8 where (31)–(40) are still valid except for replacing in (36) the $R_C || R_{\text{in3}}$ term with the input resistance of the Q4 cascode

$$R_{\text{in4}} = \frac{r_{x4} + r_{\pi 4}}{1 + h_{fe}} \approx 13.6\ \Omega \quad (43)$$

and the associated $R_{C\mu 2} C\mu_2$ time constant now decreases to 0.57 ns.

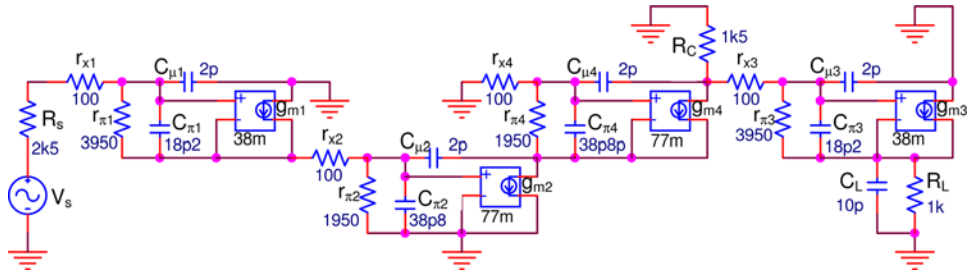

Fig. 8. Equivalent schematic in the high-frequency regime of the cascode stage of Fig. 7.

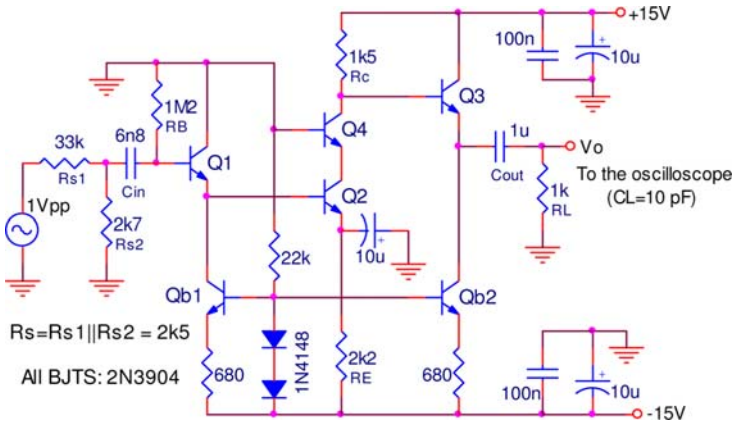

Fig. 9. Schematic of the prototype used to verify theoretical expectations.

Adding the terms due to the new cascode stage

$$R_{C\pi 4} = \frac{r_{\pi 4}}{1+h_{fe}} \approx 12.9\ \Omega \Rightarrow \tau_{C\pi 4} \approx 0.50\ \text{ns}$$
$$R_{C\mu 4} = r_{x4} + R_C||[r_{x3} + r_{\pi 3} + (1+h_{fe})R_L] \approx 1586\ \Omega \Rightarrow \tau_{C\mu 4} \approx 3.17\ \text{ns} \quad (44)$$

it can be verified that the open-circuit time-constant is now around 20.4 ns, indicating a cut-off frequency of about 7.8 MHz. Such a value would meet the speed requirement of the amplifier. Moreover, taking into account the discussion on OCTC accuracy (Section VI), such a value would underestimate the exact $\omega_{3\,\text{dB}}$ by at least 27%, having $\tau_{C\mu 1}$, $\tau_{C\pi 2}$, $\tau_{C\mu 3}$, and $\tau_{C\mu 4}$ of the same order of magnitude. A 10 MHz bandwidth would then be expected for the amplifier. A SPICE simulation, performed on the model reported in Fig. 8 shows the expected performance, indicating a bandwidth larger than 16 MHz and confirming the conservative prediction of the OCTC analysis.

To verify the design predictions, a prototype was realized following the schematic of Fig. 9. For the input and output transistors Q1 and Q3, two identical current sources were used ($I_C \approx V_{BE(ON)}/680 \approx 1\ \text{mA}$). For the cascode stage, the biasing was established by the R_B resistor connected at the Q1 base and the R_E resistor of the Q2 common emitter stage. The input signal, generated by a HP33120A, was attenuated by the $33\ \text{k}\Omega - 2.7\ \text{k}\Omega$ voltage divider to emulate the 2500 Ω source impedance.

Coupling and bypass capacitors were chosen according to the SCTC method. In such a case, the SCTC recipe was used to design the coupling capacitor values according to the specifications. First, the values of the resistors seen by the three C_{in}, C_{out} and C_E capacitors were evaluated. (Following the SCTC rule, calculations require that all the other "high-pass" capacitors be shorted.)

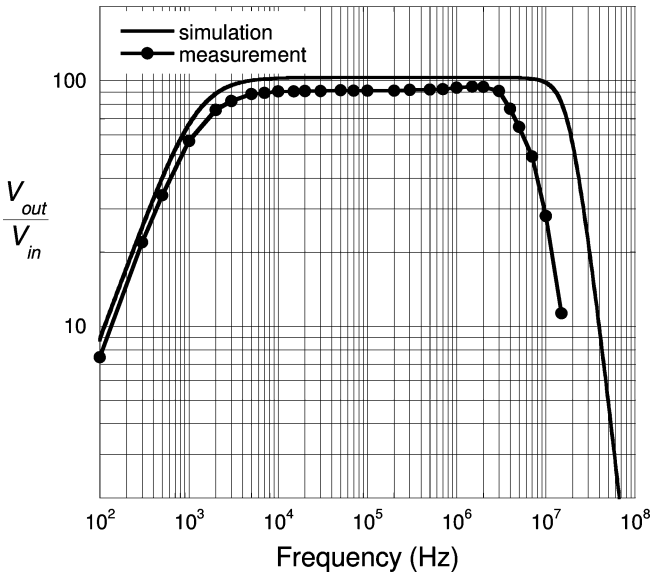

Fig. 10. Frequency response of the amplifier of Fig. 9 from simulation (continuous line) and measurements (dots).

Neglecting the contribution of the output resistance of the Qb1 and Qb2 current sources, it can be verified that

$$R_{\rm Cin} = R_S + R_B||[(r_{x1} + r_{\pi 1} + (h_{fe}+1)(r_{x2}+r_{\pi 2}))] \approx 251\ \text{k}\Omega \quad (46)$$

$$R_{\rm Cout} = R_L + \frac{R_C + r_{x3} + r_{\pi 3}}{h_{fe}+1} \approx 1037\ \Omega \quad (47)$$

$$R_{CE} = R_E|| \frac{r_{x2} + r_{\pi 2} + \frac{(R_B||R_S + r_{x1} + r_{\pi 1})}{(h_{fe}+1)}(h_{fe}+1)}{h_{fe}+1} \approx 13.8\ \Omega. \quad (48)$$

Without losing any generality in the design, $R_{CE} - C_E$ can represent the dominant cut-off component. For the 1-kHz required breakpoint, C_E would be then around 12 μF(12 $\mu \times 13.8 \approx 166\,\mu$s). In order to maintain $\omega_E = 1/R_E C_E$ dominant, cut-off contributions by $C_{\rm in}$ and $C_{\rm out}$ would be ten times lower than the 1-kHz breakpoint requirement. The capacitor values reported in Fig. 9 guarantee such a choice.

As shown in Fig. 10, experimental results are compared to SPICE simulation of the complete ac model (the circuit of Fig. 8 which includes the $C_{\rm in}$, $C_{\rm out}$, and C_E capacitors). The measured 7-MHz bandwidth is probably induced by both the presence of parasitic capacitances of the assembly and the real values of parasitic elements of the BJTs. But it is worth noting that the OCTC conservative prediction strongly agrees with the actual performance of the built circuit.

IX. Conclusion

The open-circuit and short-circuit time constant methods offer a powerful approach to estimate the bandwidth of any network of resistors, capacitors and dependent active sources. They are useful both from an analysis and a design point of view, allowing the identification of the major frequency-response bottlenecks of the system. In addition, the pessimistic nature of approximation of the bandwidth calculation performed with these methods moves toward a more realistic behavior of the circuit. Indeed, unavoidable nonidealities will strongly affect the actual performances of the circuit; exact mathematical models would not only be exceedingly difficult to implement, but would also prove inadequate, especially in the initial design process. There are several points to be aware of when using the approximated techniques described here. The methods are exact when a single energy-storage element is concerned. Indeed, as the approximation assumes, a one-pole system does not contain s^2 or higher order terms in the characteristic polynomial; the same is observed in higher order systems, when a dominant-pole condition is verified. The methods are less accurate if there is a large number of dominant poles. In addition, the accuracy is strongly degraded if zeroes or complex poles characterize the transfer function. The estimate yielded by the techniques may result overpessimistic in many circuits where *tricks* and *tips* are used to enhance as much as possible the response speed of the amplifier. (A classical example is the use of a *peaking* inductor in series with the BJT-collector load to hold up the gain at frequencies above the roll-off value, cancelling part of the effects of load-parasitic capacitances [21].) The goal of using the SCTC and OCTC methods is to get an insight into expected performance, not to obtain precise performance figures.

Acknowledgment

The authors wish to thank the reviewers of the manuscript for their really helpful comments and suggestions and to express a special thanks to Dr. Mills for her careful and professional editing work of the manuscript. In addition, the authors would like to thank S. Carta for his painstaking work regarding the mathematical formalism of the paper and to express their indebtedness to M. Girolami who has taken real professional care in reading and commenting on the work presented here.

References

[1] R. D. Thorton, C. L. Searle, D. O. Pederson, R. B. Adler, and E. J. Angelo, Jr, "Gain and bandwidth calculations: A first approximation," in *Multistage Transistor Circuits*, New York, Wiley, 1965, pp. 3–31.

[2] W. C. Elmore, "The transient response of damped linear network with particular regard to wideband amplifiers," *J. Appl. Phys.*, vol. 19, pp. 55–63, Jan. 1948.

[3] J. Rubistein, P. Penfield, and M. A. Horowitz, "Signal delay in RC tree networks," *IEEE Trans. Comput.-Aided Design*, vol. CAD-2, pp. 202–211, Jul. 1983.

[4] R. Gupta, B. Tutuianu, and L. T. Pileggi, "The Elmore delay as a bound for RC trees with generalized input signals," *IEEE Trans. Comput.-Aided Design Integr. Circuits Syst.*, vol. 16, no. 1, pp. 95–104, Jan. 1997.

[5] M. J. S. Smith, "Programmable asic interconnect," in *Application Specific Integrated-Circuits*. Boston, MA: Addison-Wesley, 1997, pp. 278–280.

[6] S. Long, "Logic Design Principles and Examples," in *VLSI Handbook*. Boca Raton, FL: CRC/IEEE, 2000, ch. 71.

[7] A. M. Davis and E. A. Moustakas, "Analysis of active RC networks by decomposition," *IEEE Trans. Circuits Syst.*, vol. CAS-27, no. 5, pp. 417–419, May 1980.

[8] R. M. Fox and S. G. Lee, "Extension of open-circuit time-constant method to allow for transcapacitances," *IEEE Trans. Circuits Syst.*, vol. 37, no. 9, pp. 1167–1171, Sep. 1990.

[9] M. T. Thompson, "Design linear circuits using OCTC calculations," *Electron. Design -Analog Appl. Issue*, pp. 41–47, Jun. 1993.

[10] M. T. Thompson, "SCTC analysis estimates low-frequency -3 dB point," *Electron. Design*, pp. 65–68, Oct. 1993.

[11] M. T. Thompson, "Network tricks aid in OCTC," *Electron. Design*, pp. 67–70, Dec. 1993.

[12] M. T. Thompson, *Intuitive Analog Circuit Design*. New York: Newnes Elsevier, 2006.

[13] R. C. Jaeger, *Microelectronic Circuit Design*. New York: McGraw-Hill, 1997.

[14] A. S. Sedra and K. C. Smith, *Microelectronic Circuits*, 5th ed. New York: Oxforfd Univ. Press, 2004.

[15] D. O. Pederson and G. H. Wilson, "Dominant zero and excess phase of a Hurwitz polynomial," *IEEE Trans. Circuit Theory*, vol. CT-11, pp. 104–108, Mar. 1964.

[16] C. L. Searle, A. R. Boothroyd, E. J. Angelo, P. E. Gray, and D. O. Pederson, *Elementary Circuit Properties of Transistors*. New York: Wiley, 1964, ch. VI.

[17] P. R. Gray and R. G. Meyer, *Analysis and Design of Analog Integrated Circuits*, 2nd ed. New York: Wiley, 1984, ch. 7.

[18] B. L. Cochrun and A. Grabel, "A method for the determination of the transfer function of electronic circuits," *IEEE Trans. Circuit Theory*, vol. CT-20, pp. 16–20, Jan. 1973.

[19] 2N3904 Datasheet, Rev. 7 2007 [Online]. Available: www.on-semi.com/PowerSolutions

[20] J. M. Miller, "Dependence of the input impedance of a three-electrode vacuum tube upon the load on the plate circuit," *Scientif. Papers of the Bur. Stand.*, vol. 15, no. 351, pp. 367–385, 1920.

[21] P. Horowitz and W. Hill, "High Frequency and High Speed Techniques," in *The Art of Electronics*, 2nd ed. Cambridge, U.K.: Cambridge Univ. Press, 1990, pp. 863–869.

Stefano Salvatori (M'00) received the M.S. degree in electronic engineering in 1992 from the University of Rome "La Sapienza," Rome, Italy, and the Ph.D. degree in electronic engineering in 1997 from the University "Roma Tre."

He collaborates, as a Research Associate, with the Department of Electronic Engineering, University of Rome Tre, since 1998. His interest is mainly focused on CVD-diamond-based UV sensors and high-energy particle detectors, but also include growth, processing, and characterization of thin-film materials for optoelectronic devices. He is primarily involved in the development of single- or multichannel front-end electronics for low-level signal sensors. He is a coauthor of more than 50 papers published on international scientific journals.

Gennaro (Rino) Conte received the degree in physics from the University of Rome "La Sapienza," Rome, Italy.

He serves as a Professor in Analog Electronics with the Department of Electronic Engineering, University "Roma Tre," since 1998. Prior to this, he was a Member of the Technical Staff of the ENEA, National Agency for Renewable Energies, and a manager at the ENI Research Centre, Monterotondo (Rome). He has conducted research on solid-state devices for over 20 years and his current research concentrates on transport properties of materials, UV and X-ray sensor devices, and high-frequency MESFETs based on polycrystalline diamond.